Temperature Dependence of CO-Tolerant Hydrogen Oxidation Reaction Activity at Pt, Pt−Co, and Pt−Ru Electrodes

Hiroyuki Uchida,[†] Kenji Izumi,[†] and Masahiro Watanabe*[,‡]

Interdisciplinary Graduate School of Medicine and Engineering and Clean Energy Research Center, University of Yamanashi, Takeda 4, Kofu 400-8510, Japan

Received: July 4, 2006; In Final Form: August 19, 2006

The temperature dependence of CO-tolerant H_2 oxidation reaction (HOR) activity at Pt, Pt−Co, and Pt−Ru electrodes in 0.1 M $HClO_4$ solution was examined with a channel flow electrode at 30 to 90 °C. The kinetically controlled current density (j_K) for the HOR at Pt decreased seriously at CO overage (θ_{CO}) >0.6 in the whole temperature range examined. In contrast, the Pt−Ru alloy exhibited an excellent CO tolerance: only 15% reduction in j_K even at $\theta_{CO} = 0.6$ and 30 °C. The Pt−Co alloy also showed moderate CO tolerance up to 70 °C. It was found for these alloys that the CO adsorption rate was much slower than that of Pt and the HOR sites were not so rigidly blocked by adsorbed CO due to its enhanced mobility, resulting from their modified electronic structure of surface Pt sites. The activation energies for the apparent rate constants for the HOR were as low as 3.0 and 5.3 kJ mol^{-1} at Pt and Pt−Ru, respectively, indicating that the high-temperature operation increases CO-free HOR sites as well as enhancing the HOR kinetics.

1. Introduction

Polymer electrolyte fuel cells (PEFCs) have attracted great interest as a primary power source for electric vehicles or residential co-generation systems.[1] Nanosized platinum particles supported on high surface area carbon substrates (Pt/CB) have been used as the catalyst for both the anode and the cathode. When pure hydrogen is used as the fuel, the overpotential for the hydrogen oxidation reaction (HOR) at the Pt anode is negligibly small. In contrast, the Pt catalyst operating with reformates is seriously poisoned by trace amounts of carbon monoxide; CO molecules strongly adsorbed on the active sites block the HOR.[2,3] Thus, extensive efforts have been made to develop CO-tolerant anode catalysts and on alteration of cell operating conditions to suppress the effects of CO in the fuel stream, such as anode air-bleeding.

To evaluate the catalytic activity or to investigate the reaction mechanism, planar electrodes with well-defined characteristics such as surface area, surface and bulk compositions, and crystal structure have often been examined in acidic electrolyte solutions. An appreciable improvement of the CO tolerance has been found at Pt with adatoms such as Ru, Sn, or As,[4−10] Pt-based alloys Pt−M (M = Ru, Rh, Os, Sn, etc.),[11−17] and Pt with oxides (RuO_xH_y).[18,19] Recently, we found new CO-tolerant catalysts by alloying Pt with a second nonprecious metal (Pt−Fe, Pt−Co, Pt−Ni, etc.).[20−27] These alloys exhibited excellent CO-tolerant HOR activity similar to Pt−Ru alloy in H_2 containing 100 ppm CO at room temperature. By using X-ray photoelectron spectroscopy (XPS),[23−25] in situ scanning tunneling microscopy (STM),[26] and electrochemical quartz crystal microbalance (EQCM),[27] it was found that the nonprecious metal atoms leached out into an acidic electrolyte solution and a Pt skin layer with a modified electronic structure was formed on the alloy surface.

It is essential to evaluate precisely the effect of CO coverage on the kinetically controlled current density j_K for the HOR at these electrodes. For this purpose, a rotating disk electrode (RDE) is one of the powerful tools employed so far. With a view of PEFC operation, the CO poisoning can be mitigated by using the Pt alloys and/or elevating the operating temperature. However, the temperature dependencies of the HOR activities in the presence of CO have been scarcely reported for the practical temperature range of PEFC, i.e., room temperature to 90 °C. Schmidt et al. applied a thin-film RDE technique in both the HOR and the oxygen reduction reaction (ORR), in which Pt/CB catalysts were attached on a glassy carbon disk electrode by means of a thin Nafion film.[28,29] They reported kinetics of CO oxidation and the HOR on Pt/CB in a relatively large overpotential region and at 60 to 80 °C, but the temperature dependence of the intrinsic HOR activity was not shown.[28] One of the difficulties is a correction of the change in H_2 concentration in the electrolyte solution at the RDE cell that is open to the atmosphere at elevated temperatures. Recently, we demonstrated that the use of a channel flow double electrode (CFDE) cell can provide precise data on an apparent rate constant k_{app} and apparent activation energy for the ORR at Pt or Pt-alloy electrodes at 20 to 90 °C,[30,31] as well as at Nafion-coated film electrodes of Pt/CB at 30 to 110 °C.[32] The CFDE cell can be operated as a closed system with controlled reactant concentration, for example, dissolved O_2 for the ORR and H_2 for the HOR. From the hydrodynamic voltammograms under various laminar flow rates of the electrolyte solution, the kinetically controlled current density j_K at the planar working electrode has been evaluated by a well-defined Levich equation. At the collecting electrode located at the downstream of the working electrode, the H_2O_2 production rate, a byproduct in the ORR, was successfully quantified.

In the present work, by using the channel flow electrode (CFE) cell, we have evaluated the j_K and k_{app} for the HOR at Pt, Pt−Co, and Pt−Ru planar electrodes with various CO coverage in 0.1 M $HClO_4$ solution as a function of temperature

* To whom correspondence should be addressed. Phone: +81-55-220-8620. Fax: +81-55-254-0371. E-mail: m-watanabe@yamanashi.ac.jp.
† Interdisciplinary Graduate School of Medicine and Engineering.
‡ Clean Energy Research Center.

10.1021/jp064190x CCC: $33.50
Published on Web 09/26/2006

from 30 to 90 °C. We have chosen Pt−Co and Pt−Ru alloys, since they were reported to exhibit excellent CO tolerance with different surface states in the acidic solution; the precious (corrosion-resistant) metal Ru remained at the Pt−Ru surface, whereas a Pt skin layer was formed at Pt−Co by a dissolution of Co followed by a rearrangement of remaining Pt atoms.[21−27] We demonstrate that the pure Pt electrode exhibits the highest HOR activity for CO-free condition in the whole temperature range, but a Pt−Ru alloy exhibits the highest CO-tolerant HOR activity. The mechanism of the CO tolerance is also discussed.

2. Experimental Section

The experimental setup of the channel flow electrode (CFE) cell and flow circuit of electrolyte solution was the same as that of our previous work,[30,31] except that the collecting electrode was not operated for the HOR. The CFE cell was made of Kel-F blocks and a Teflon sheet, resistant to hot acid electrolyte solution. The thickness of the solution flow channel was 0.5 mm. As the working electrode, pure Pt, Pt−Co, and Pt−Ru alloy films (0.1 cm × 0.4 cm, geometric area $A = 0.04$ cm^2) were prepared on a gold substrate by Ar-sputtering (SH-33D, ULVAC Co Ltd.) a Pt target together with a Co or Ru target at room temperature. The thickness of the films was controlled gravimetrically to about 0.1 μm. The resulting alloy compositions determined by X-ray fluorescent analysis (EDX-800, Shimadzu) were $Pt_{51}Co_{49}$ and $Pt_{54}Ru_{46}$ in atomic ratio. The crystallographic structures of these alloys were examined by grazing incidence ($\theta = 1°$) X-ray diffraction (GIRD). GIRD patterns of these alloys indicated the formation of a solid solution with a face-centered cubic crystal structure. A platinum wire was used as a counter electrode. The reversible hydrogen electrode, kept at the same temperature as that of the cell (t, °C), was used as the reference electrode [denoted as RHE(t)]. All the electrode potentials in this paper will be referenced to the RHE(t).

The electrolyte solution of 0.1 M $HClO_4$ was prepared from reagent grade chemicals (Kanto Chemical Co.) and Milli-Q water (Milli-Pore Japan Co. Ltd.) and purified in advance with conventional pre-electrolysis methods.[33,34] The electrolyte solution was saturated with N_2, pure H_2, and 0.100% CO (H_2-balance, Sumitomo Seika, Japan) bubbling in three separate Teflon reservoirs, respectively, for at least 1 h prior to the electrochemical measurements. The total pressure of the gas phase in each electrolyte solution reservoir was kept slightly higher than atmospheric pressure (1 atm) at 30 to 90 °C (see the Supporting Information). The diffusion coefficient D of dissolved hydrogen was calculated based on the Stokes−Einstein equation. The dissolved hydrogen concentration [H_2] was calculated by using Henry's law, but a correction was made based on the measured limiting current (Table A2 and Figure A1 in the Supporting Information).

A potentiostat (ALS 700A, BAS Inc.) was used for the electrochemical measurements. Prior to the HOR experiments at each temperature, the working electrode was electrochemically stabilized by repetitively sweeping the potential from 0.05 to 1.00 V for pure Pt and Pt−Co, and from 0.05 to 0.80 V for Pt−Ru at the sweep rate of 0.10 V s^{-1} in 0.1 M $HClO_4$ solution deaerated with N_2 gas until the voltammogram reached a steady state (typically 20 cycles). The electrochemically active area of the working electrode $S°$ (CO-free surface) was determined from the hydrogen desorption charge in the positive-going potential scan (0.10 V s^{-1}) from 0.05 to 0.40 V in N_2-saturated 0.1 M $HClO_4$ (without solution flow), referred to $\Delta Q_H° = 0.21$ mC cm^{-2} adopted conventionally for a clean polycrystalline platinum.[33] The HOR activity of the CO-free electrode surface was examined by recording hydrodynamic voltammograms under a flow of H_2-saturated 0.1 M $HClO_4$ solution (mean flow rate = 10−50 cm s^{-1}) in the potential range from 0 to 0.10 V at the potential sweep rate of 0.5 mV s^{-1}. At the slow scan rate, the current hysteresis of the positive-going and negative-going scans was negligibly small. The current−potential relationship measured in such a condition shows "the real activity of the electrocatalyst examined under steady-state conditions".

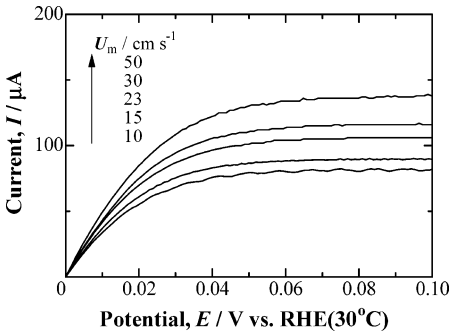

Figure 1. Hydrodynamic voltammograms for the HOR at Pt working electrode in H_2 saturated 0.1 M $HClO_4$ at 30 °C measured at the potential sweep rate of 0.5 mV s^{-1} and various mean flow rates of the solution, U_m, from 10 to 50 cm s^{-1}.

Carbon monoxide was adsorbed on the working electrode by flowing 0.1 M $HClO_4$ solution saturated with 0.100% CO (H_2-balance) at the mean flow rate of 50 cm s^{-1} for various time intervals (t_{ad}) with keeping the potential at 0.050 V. After changing the solution thoroughly to N_2-saturated 0.1 M $HClO_4$, the CO coverage (θ_{CO}), defined by eq 6 in section 3.3, was just checked, without CO desorption, by measuring the decrease in the hydrogen desorption charge ΔQ_H in a potential scan from 0.05 to 0.40 V at 0.10 V s^{-1}. Then, the HOR activity at the CO-adsorbed electrode surface was examined by recording hydrodynamic voltammograms under a flow of pure H_2-saturated 0.1 M $HClO_4$ solution in the same manner as described above. Finally, a CO-stripping voltammogram was taken to determine both the ΔQ_H and the CO oxidation charge (ΔQ_{CO}) at the sweep rate of 0.10 V s^{-1} in N_2-saturated 0.1 M $HClO_4$.

3. Results and Discussion

3.1. Hydrodynamic Voltammetry for HOR at the CO-Free Condition. Figure 1 shows hydrodynamic voltammograms for the HOR at the CO-free Pt working electrode in H_2-saturated 0.1 M $HClO_4$ solution at 30 °C at a mean solution flow rate of 10 to 50 cm s^{-1}. The HOR currents at the Pt working electrode commence at 0.00 V vs RHE(30 °C) and reach diffusion limits at approximately around 0.05 V. Thus, the facile HOR is confirmed at the CO-free Pt electrode.

The kinetically controlled current I_K at a given potential E is determined from the hydrodynamic voltammogram in the CFE by using the following equation[35]

$$1/I = 1/I_K + 1/I_L = 1/I_K + 1/\{1.165nF[H_2]w(U_m D^2 x_1^2/h)^{1/3}\} \quad (1)$$

where n is the number of electrons transferred, F is the Faraday constant, [H_2] is the H_2 concentration in the bulk of electrolyte solution, w is the width of the working electrode, U_m is the mean flow rate of the electrolyte solution, D is the diffusion coefficient of H_2, x_1 is the length of the working electrode in the solution flow direction, and h is the half thickness of the electrolyte flow over the electrodes. Figure 2 shows plots of

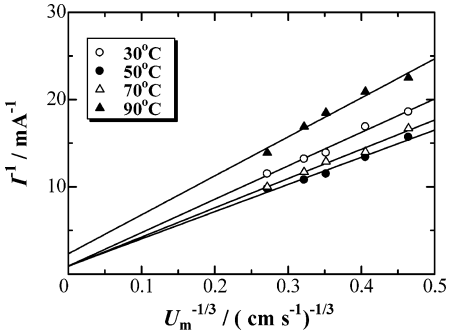

Figure 2. I^{-1} vs $U_m^{-1/3}$ plots at 0.020 V vs RHE(t) obtained from hydrodynamic voltammograms at Pt working electrode in H_2 saturated 0.1 M $HClO_4$ solution in the temperature range from 30 to 90 °C. The solid line is the least-squares fitting.

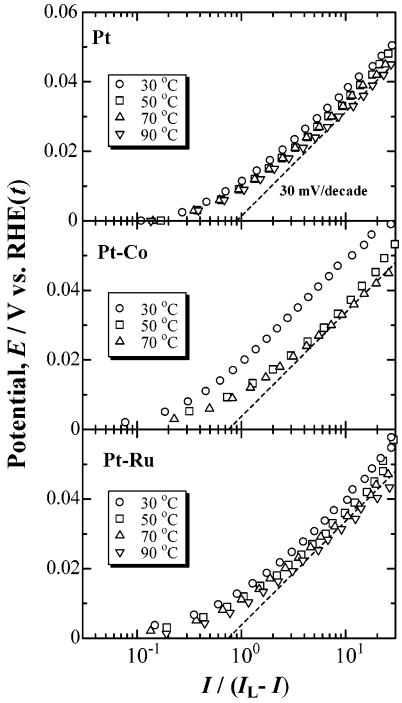

Figure 3. Tafel plots for the HOR at Pt, $Pt_{51}Co_{49}$, and $Pt_{54}Ru_{46}$ working electrodes in H_2 saturated 0.1 M $HClO_4$ solution (U_m = 30 cm s^{-1}) at 30 to 90 °C. Dashed line shows the slope of 30 mV decade^{-1}.

I^{-1} vs $U_m^{-1/3}$ obtained at E = 0.020 V and t = 30 to 90 °C. Linear relationships are seen at all the temperatures. The number of electrons n calculated from the slope with eq 1 was found to be approximately 2, which agrees well with the theoretical one for the HOR. By extrapolating $U_m^{-1/3}$ to 0 (infinite flow rate), we determined the kinetically controlled HOR current I_K at 30 to 90 °C. The values of I_K are, however, apparently constant at 30 to 70 °C, and decrease at 90 °C. This is because the increase in the catalytic activity is canceled by the steep reduction in $[H_2]$, i.e., the value of $[H_2]$ at 90 °C is about one-third of that at 30 °C (Table A2 in the Supporting Information).

A change in the HOR activity with temperature is illustrated by mass-transfer-corrected Tafel plots, E vs $\log[I/(I_L - I)]$, in Figure 3. At all the electrodes, the Tafel lines shift to less positive potential with elevating temperature; the HOR activity clearly increases with temperature. The Tafel slope at 30 to 90 °C for pure Pt electrode was ca. 30 mV/decade at E > 0.02 V, which is in accord with that reported for the smooth Pt electrode at room temperature in 0.5 M H_2SO_4.[36] For such a value of the Tafel slope, dissociative adsorption of H_2 is generally accepted as the rate-determining step (rds) for the HOR.[36]

$$H_2 + 2Pt \rightarrow 2Pt{-}H_{ad} \qquad \text{rds} \qquad (2)$$

$$2Pt{-}H_{ad} \rightarrow 2H^+ + 2e^- + 2Pt \qquad \text{fast} \qquad (3)$$

Because almost the same Tafel slope of ca. 30 mV/decade is seen for Pt−Co and Pt−Ru electrodes in Figure 2, the rds at these electrodes is certainly the same as that of pure Pt. The Tafel slopes at several electrodes have been summarized by Conway et al.[36] Some inconsistent values among these summarized values may be ascribed to a narrow Tafel region due to the facile HOR kinetics (see Figures 1 and 3), which makes it difficult to accurately determine the slope. An appropriate correction for the mass transfer of dissolved H_2 is essential, which can be accomplished by using the RDE or the CFE, used in the present work.

3.2. Hydrogen Oxidation Rate Constants and Activation Energies. We have calculated an apparent rate constant, k_{app}, corrected for the change in $[H_2]$ with temperature to discuss the temperature dependence of the HOR activity. We employ the kinetic current density, j_K, defined as the kinetic current I_K per active area of the electrode $S°$ (CO-free surface).

$$j_K = I_K/S° \qquad (4)$$

We assumed the original number of HOR active sites being equal to that of the hydrogen adsorbing sites, irrespective of pure Pt, Pt skin on Pt−Co alloy, or Pt−Ru alloy, although the HOR active sites may not always be the same as those for underpotentially deposited hydrogen, H_{upd}.[37] For the HOR reaction in eqs 2 and 3, we can use the following equation,

$$j_K/2F = k_{app}[H_2] \qquad (5)$$

Figure 4 shows Arrhenius plots of k_{app} at 0.020 V. For a CO-free surface; the value of k_{app} at the Pt electrode is the highest in the whole temperature range. The Pt−Co and Pt−Ru exhibited almost comparable k_{app} at 30 to 50 °C. The apparent activation energies at Pt, Pt−Co, and Pt−Ru at 30 to 70 °C were as low as 3.0, 4.2, and 5.3 kJ/mol, respectively. Hence, increasing the operating temperature does not lead to significant enhancement in the HOR kinetics. For example, the k_{app} for the HOR on Pt at 90 °C was two times higher than that at 30 °C, whereas the k_{app} for the ORR increased about 1 order of magnitude from 30 to 90 °C.[30] However, for both pure Pt and Pt−Ru electrodes at 90 °C, some upward shift of k_{app} from the Arrhenius relation may suggest further enhanced kinetics in the higher temperature region >100 °C. Such a curvature was very reproducibly observed for these electrodes irrespective of elevating or lowering the temperature, although the reason for the curvature is not clear at the present stage. In contrast, much larger activation energies at Pt (17 kJ/mol) and $Pt_{50}Ru_{50}$ alloy (19 kJ/mol) were reported for the HOR in hot concentrated H_3PO_4 at 120 to 160 °C,[12] where the HOR rate might be suppressed by specifically adsorbed phosphate anions especially at the lower temperature region.

3.3. Adsorption of CO at Pt, Pt−Ru, and Pt−Co Electrodes. Carbon monoxide was adsorbed on the working electrode by the procedure described in the Experimental Section. Figure 5A shows typical CO-stripping voltammograms at Pt, Pt−Co, and Pt−Ru electrodes measured in N_2-saturated 0.1 M $HClO_4$ solution at 30 °C. The hydrogen desorption currents at 0.05 to 0.40 V are reduced by the occupation of Pt sites with adsorbed CO (CO_{ad}). We defined the CO coverage (θ_{CO}) as the site occupation by the following equation, regardless

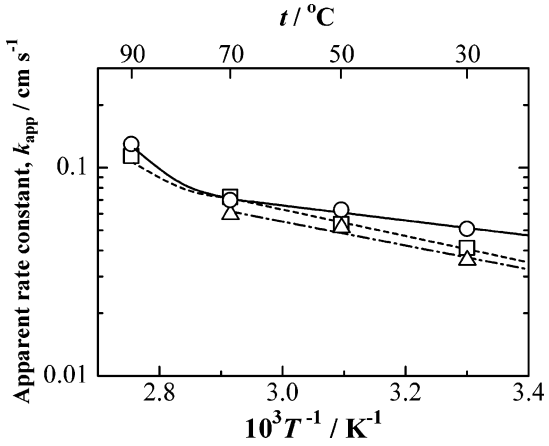

Figure 4. Arrhenius plots for the apparent rate constant k_{app} for the HOR (CO-free) at (○) Pt, (△) $Pt_{51}Co_{49}$, and (□) $Pt_{54}Ru_{46}$ working electrodes at 0.020 V vs RHE(*t*).

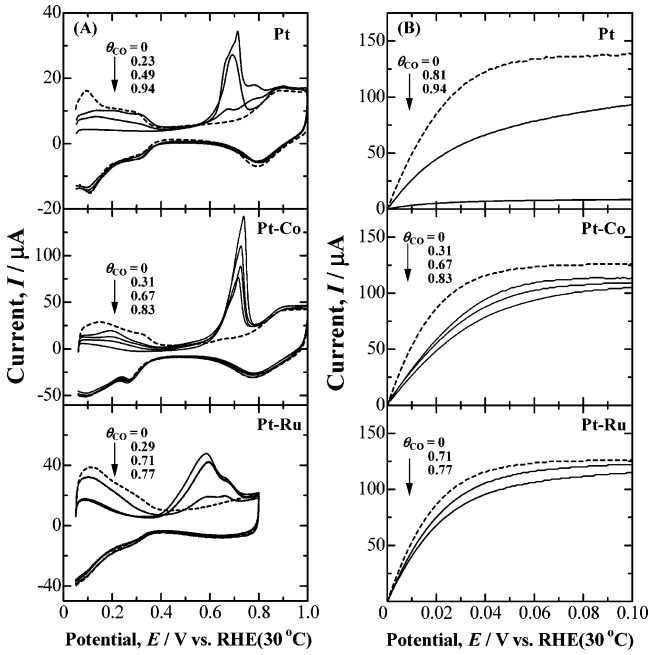

Figure 5. (A) CO-stripping voltammograms at Pt, $Pt_{51}Co_{49}$, and $Pt_{54}Ru_{46}$ electrodes measured in N_2 saturated 0.1 M $HClO_4$ solution at 30 °C and potential sweep rate of 0.10 V s^{-1}. The dotted line shows CV at the CO-free surface. (B) Changes in the hydrodynamic voltammograms for the HOR at these electrodes with various θ_{CO}. The HOR voltammograms were measured in H_2 saturated 0.1 M $HClO_4$ solution at 30 °C before recording CO-stripping voltammograms.

of the type of CO_{ad}, e.g., linear (on-top), bridged, or the derivatives,

$$\theta_{CO} = 1 - (\Delta Q_H/\Delta Q_H^\circ) \quad (6)$$

where ΔQ_H and ΔQ_H° are the hydrogen-desorption charges with and without CO_{ad}, respectively. Figure 5B shows changes in the hydrodynamic voltammograms for the HOR at these electrodes with various θ_{CO}, which were measured in H_2-saturated 0.1 M $HClO_4$ solution in the potential range from 0 to 0.10 V and at 30 °C. It is clear that pure Pt electrode lost the HOR activity dramatically at high θ_{CO}, whereas such a CO poisoning was mitigated at Pt−Co and Pt−Ru electrodes.

In Figure 5A, the CO_{ad} oxidation commences at about 0.5 V in a positive-going potential scan on the pure Pt electrode. The Pt−Co alloy electrode exhibits almost the same onset potential, i.e., no specific enhancement of direct CO_{ad} oxidation.[23,24,27] In

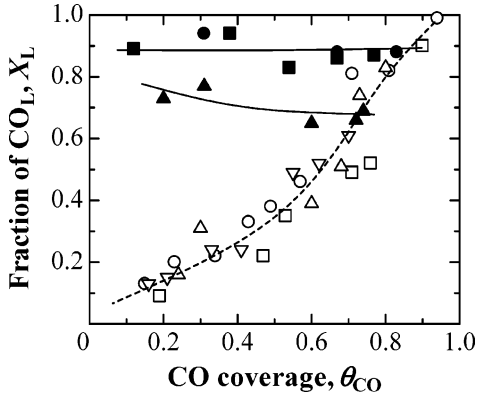

Figure 6. The fraction of linearly bonded CO (X_L) as a function of θ_{CO} at pure Pt (open symbols) and $Pt_{51}Co_{49}$ (closed symbols) electrodes. Temperature: 30 (○, ●), 50 (□, ■), 70 (△, ▲), and 90 °C (▽).

contrast, the CO_{ad} oxidation at the Pt−Ru commences at 0.4 V and the current steeply rises to reach the peak at 0.6 V. As proposed by Watanabe et al.[4] and recently confirmed by in situ FTIR spectroscopy,[38] the CO_{ad} oxidation at Pt sites is facilitated by oxygen species adsorbed at Ru sites (Ru−OH), in the so-called "bifunctional mechanism". However, the activity for the CO_{ad} oxidation is not directly related to the CO-tolerant HOR activity at such a less positive potential, because CO_{ad} cannot be removed from the surface at $E < 0.1$ V even on Pt−Ru. The most essential point is why the HOR can proceed at Pt−Co or Pt−Ru alloy electrodes without significant reduction in the activity even with high θ_{CO} levels, as seen in Figure 5B.

3.4. Type of CO_{ad} at Pt and Pt−Co Electrodes. One of the interesting points is whether the type of CO_{ad} changes with alloying and with temperature. Since θ_{CO} is simply the fraction of surface sites at which hydrogen atoms cannot adsorb, it is not always proportional to the total amount of CO_{ad} (N_{CO}) if CO molecules adsorb in multibonding form (bridged or 3-fold).[3,39] The value of N_{CO} is calculated from the two-electron oxidation charge of CO_{ad} (ΔQ_{CO-ox}),

$$N_{CO} = \Delta Q_{CO-ox}/2F = (\Delta Q_{CO} - \Delta Q^\circ)/2F \quad (7)$$

where ΔQ_{CO} and ΔQ° are the charges for CO_{ad} oxidation region in the positive-going scan with and without CO_{ad}, respectively. The average number of Pt sites occupied by one CO_{ad} ($n_{Pt/CO}$) is calculated by the following equation,

$$n_{Pt/CO} = 2\theta_{CO}\Delta Q_H^\circ/\Delta Q_{CO-OX} \quad (8)$$

Here, we simply assume that CO_{ad} is either linear-type (CO_L with $n_{Pt/CO} = 1$) or bridged-type (CO_B with $n_{Pt/CO} = 2$). The fraction of CO_L and CO_B, denoted as X_L and X_B, can be expressed as follows,[3,39]

$$X_L + X_B = 1 \quad (9)$$

$$n_{Pt/CO} = X_L + 2X_B \quad (10)$$

Then, we obtain

$$X_L = 2 - n_{Pt/CO} \quad (11)$$

$$X_B = n_{Pt/CO} - 1 \quad (12)$$

Figure 6 shows change in X_L with θ_{CO}. At pure Pt electrode, X_L increases with increasing θ_{CO}. CO_L is predominant at high $\theta_{CO} > 0.9$, consistent with previous results with RDE[3] and in situ FTIR spectroscopy[40,41] at room temperature. In the present

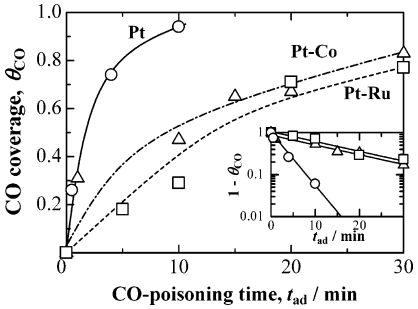

Figure 7. Time course of increase in θ_{CO} (○) Pt, (△) $Pt_{51}Co_{49}$, and (□) $Pt_{54}Ru_{46}$ on exposure to 0.1 M $HClO_4$ solution saturated with 0.100% CO (H_2-balance) at 0.050 V at 30 °C. The inset shows plots of $\log(1 - \theta_{CO})$ against t_{ad}, in which the solid line is the least-squares fitting.

research, however, we are the first to find that such a behavior is almost independent of the temperature from 30 to 90 °C. It is very interesting at Pt−Co that CO_L is dominant over the whole θ_{CO}. This is consistent with our in situ FTIR results for Pt skin on Pt−Fe alloy and can be ascribed to its modified electronic state by underlying alloy.[23,24] With elevating temperature to 70 °C, the X_L decreases slightly due to a change in the surface structure at Pt−Co as described below, but it is still larger than pure Pt. Thus, a clear difference in the adsorption state of CO is demonstrated between Pt and Pt−Co. For the Pt−Ru alloy, we do not discuss X_L because it was difficult to calculate $n_{Pt/CO}$ accurately due to the oxide formation current in the blank CV (Figure 5A).

3.5. CO Adsorption Rates. It was also found that the time course of increase in the θ_{CO} at Pt−Ru or Pt−Co on exposure to CO was quite different from that of pure Pt. Figure 7 shows typical results at 30 °C, and data sets at other temperatures are shown in the Supporting Information. The θ_{CO} at Pt−Ru is suppressed down to 0.3 at $t_{ad} = 10$ min and 30 °C, whereas θ_{CO} at Pt reaches 0.95 under the same conditions. The Pt−Co alloy also shows a slow CO adsorption at 30 to 70 °C. Assuming a simple Langmuir-type process for the CO adsorption, the adsorption rate is proportional to the number of free sites[3]

$$-\log(1 - \theta_{CO}) = k_{ad}[CO]^{\alpha} t_{ad} \qquad (13)$$

where k_{ad}, [CO], and α are the adsorption rate constant, the CO concentration dissolved in the solution, and the reaction order for CO adsorption, respectively. As shown in the inset, good linear relationships are seen between $\log(1 - \theta_{CO})$ and t_{ad}. The slope of each line, corresponding to $k_{ad}[CO]^{\alpha}$, is plotted as a function of temperature in Figure 8A. The values of $k_{ad}[CO]^{\alpha}$ at Pt−Co and Pt−Ru are comparable, and are smaller than that of pure Pt: ca. $^1/_5$ at 30 °C. With elevating temperature, the $k_{ad}[CO]^{\alpha}$ at Pt decreases markedly, while the alloys show only small reduction. For pure Pt electrode at room temperature, the value of α was found to be unity.[3] By employing $\alpha = 1$ and values of [CO] shown in the Supporting Information, we estimated k_{ad} values at different temperatures. Because the k_{ad} at pure Pt decreases slightly with temperature as shown in Figure 8B, a suppression of the CO adsorption rate at Pt may not be so expected up to 90 °C when [CO] is constant. In contrast, those at both alloys are lower than those of pure Pt at all temperatures, although it may be difficult to understand the positive temperature coefficients of k_{ad} at the alloys. The unknown factor is α for these alloys. An inspection for these values shows that the temperature coefficient of k_{ad} becomes zero if α is $^1/_3$. Thus, one of the distinct factors for the CO-tolerant HOR at Pt−Co and Pt−Ru is the deceleration of the CO adsorption rate.

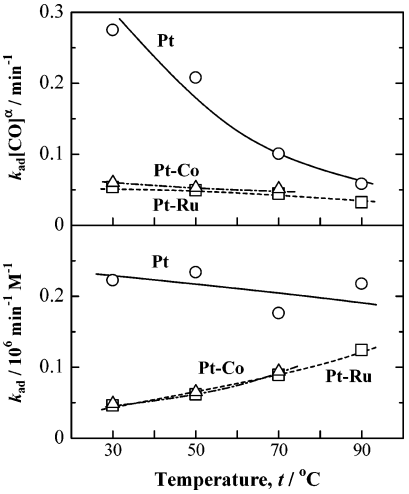

Figure 8. (A) Dependence of $k_{ad}[CO]^{\alpha}$ on the temperature at Pt, $Pt_{51}Co_{49}$, and $Pt_{54}Ru_{46}$, where $k_{ad}[CO]^{\alpha}$ was obtained from the slope of insets shown in Figure 7 and Figure S-2 (Supporting Information). (B) Plots of adsorption rate constants k_{ad} as a function of temperature, assuming $\alpha = 1$.

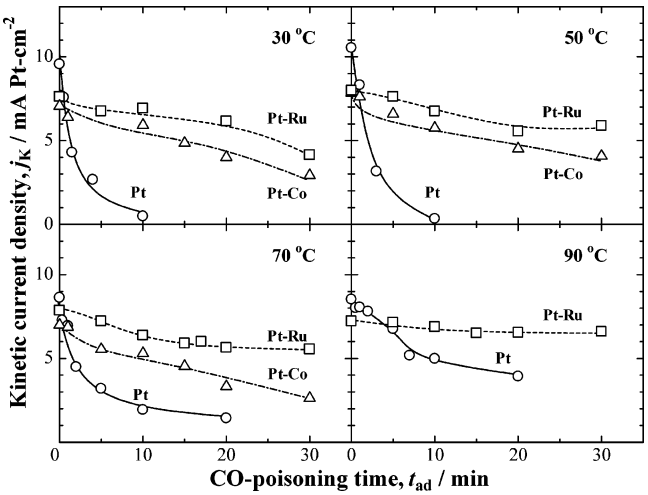

Figure 9. Change in the kinetically controlled current density j_K at 0.020 V with CO-poisoning time (t_{ad}) for Pt, $Pt_{51}Co_{49}$, and $Pt_{54}Ru_{46}$ electrodes. After each electrode was exposed to 0.1 M $HClO_4$ solution saturated with 0.100% CO (H_2-balance) at 0.050 V for a given period t_{ad}, the j_K at 0.020 V was evaluated in H_2 saturated 0.1 M $HClO_4$ solution, followed by the determination of θ_{CO} in N_2 saturated 0.1 M $HClO_4$.

3.6. CO-Tolerant HOR Activities at Pt, Pt−Co, and Pt−Ru Electrodes. The kinetically controlled current density, j_K, for the HOR (defined by eq 4) in the presence of CO_{ad} at these electrodes is compared. Figure 9 shows changes in the j_K at 0.020 V with CO-poisoning time (t_{ad}). For the pure Pt electrode operated at low temperatures of 30 to 50 °C, the value of j_K steeply decreases and reaches nearly zero after 10 min of poisoning time. The CO poisoning at pure Pt slows down with elevating temperature; the apparent loss in j_K is approximately 40% after 10 min at 90 °C. However, as discussed above, this is mainly ascribed to a decrease in [CO] at high temperature. Hence, the CO tolerance at pure Pt cannot be improved markedly by high-temperature operation up to 90 °C, although Ross et al. reported that pure Pt was the most active in comparison with various Pt−Ru alloys at 160 °C.[12] At 30 to 90 °C in Figure 9, the Pt−Ru alloy keeps the high HOR activity;

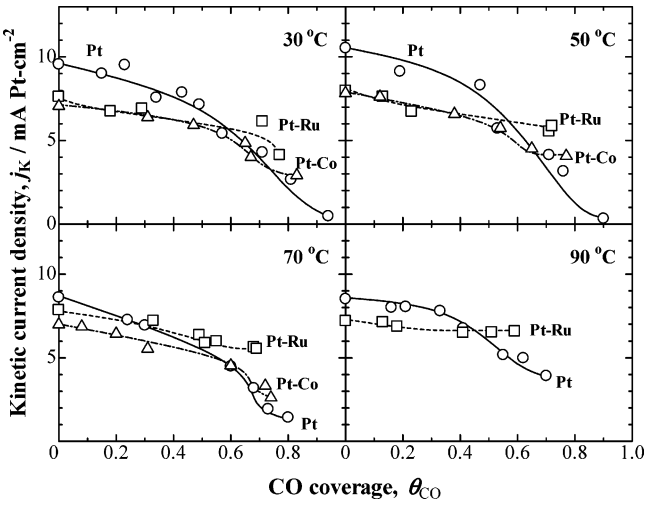

Figure 10. Dependence of j_K at 0.020 V on θ_{CO} for Pt, $Pt_{51}Co_{49}$, and $Pt_{54}Ru_{46}$ electrodes in H_2 saturated 0.1 M $HClO_4$ solution.

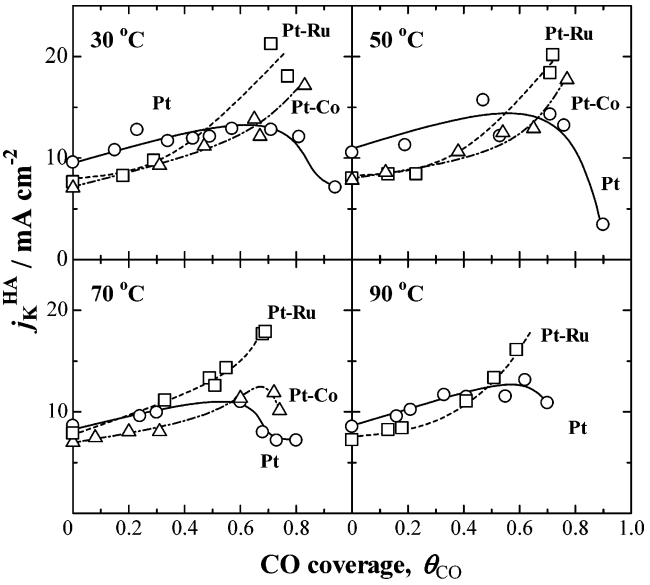

Figure 11. Dependence of j_K^{HA} [$=j_K/(1 - \theta_{CO})$] at 0.020 V on θ_{CO} for Pt, $Pt_{51}Co_{49}$, and $Pt_{54}Ru_{46}$ electrodes in H_2 saturated 0.1 M $HClO_4$ solution.

the reduction in the j_K is as low as 9% after $t_{ad} = 30$ min at 90 °C. The Pt−Co alloy shows moderate CO tolerance at 30 to 70 °C, i.e., superior to Pt but inferior to Pt−Ru.

Next, we focus on how the dependence of j_K on θ_{CO} changes with the electrode material and temperature. As shown in Figure 10, the value of j_K at the Pt electrode decreases gradually with increasing θ_{CO} up to ca. 0.4 at all temperatures. However, it decreases steeply at $\theta_{CO} > 0.6$ and reaches nearly zero at $\theta_{CO} > 0.9$. Such a CO-poisoning property of Pt is consistent with those measured at room temperature.[3,42,43] In contrast, the Pt−Ru alloy exhibits excellent CO-tolerant HOR activity at 30 to 90 °C. The CO tolerance at Pt−Ru is somewhat improved with elevating temperature. For example, at $\theta_{CO} = 0.5$, the reductions in j_K values are 15% at 30 °C and 9% at 90 °C, respectively. At low θ_{CO} region less than 0.5, the pure Pt exhibited higher j_K than those at alloys, but such a j_K could not be sustained due to the fast CO adsorption rate described above.

The reason for such different behaviors mentioned above can be well understood by replotting these data into Figure 11, where the current per remaining hydrogen-adsorption sites free from CO_{ad}, $j_K^{HA} = j_K/(1 - \theta_{CO})$, is displayed as a function of θ_{CO}. If the HOR active sites are tightly blocked by the immobile CO_{ad}, the value of j_K^{HA} should be constant independent of θ_{CO}. The j_K^{HA} at pure Pt increases slightly up to θ_{CO} of 0.6, but it decreases rapidly at high θ_{CO}. Such an increase in the j_K^{HA} at low θ_{CO} suggests that Pt sites were not blocked rigidly by CO_{ad} at $\theta_{CO} < 0.6$. The steep decrease in the j_K or j_K^{HA} at high $\theta_{CO} > 0.7$ is certainly due to a decrease in neighboring two active (CO-free) sites required for H_2 dissociative adsorption in the rds (eq 2), since most of CO molecules are linearly adsorbed at such high θ_{CO},[3,40,41] resulting in isolated Pt sites.

It is striking that the j_K^{HA} at Pt−Ru increases with θ_{CO} at all temperatures, doubling in value at $\theta_{CO} = 0.7$ compared with that at $\theta_{CO} = 0$. The dependence of j_K^{HA} on θ_{CO} at Pt−Co alloy is also similar to that of Pt−Ru up to 50 °C. This indicates that the HOR sites on Pt−Ru and Pt−Co are not so rigidly blocked by CO_{ad} due to its enhanced mobility. Considering that CO_{ad} on Pt−Ru and Pt−Co is not oxidized at such a low potential region $E < 0.1$ V, it is reasonable to ascribe the increase in the mobility of CO_{ad} (weakening of the Pt−CO interaction) to an electronic effect caused by the second element Ru in Pt−Ru and by underlying alloy of Pt−Co.[21,23,24] Recently, by using X-ray photoelectron spectroscopy combined with an electrochemical cell, we have found clear and direct evidence for the modified electronic structures of surface Pt atoms in Pt−Co and Pt−Ru, resulting in a positive core level shift of $Pt4f_{7/2}$ by 0.19 and 0.39 eV, respectively.[25] It was also revealed that the surface core level shifts for the CO adsorption decreased in the order of Pt > Pt skin-layer on Pt−Co alloy > Pt−Ru alloy, indicating that Ru and Co are effective elements to weaken the strength of the Pt−CO bond. In addition to the electronic effect, the high-temperature operation could result in an enhanced mobility of CO_{ad} together with an activation of the HOR kinetics to some extent (see Figure 4).

As shown in Figures 10 and 11, the CO tolerance at Pt−Co degraded at 70 °C. Its HOR activity at a given θ_{CO} is close to that of pure Pt, although the deceleration effect on the CO adsorption rate was observed at 70 °C (Figure 8). Such a "deactivated" electrode cannot recover the original CO tolerance observed at the low temperature region. This is certainly ascribed to a dealloying of the nonprecious metal component (Co) in a hot acid solution, resulting in the formation of a thicker Pt layer, the electronic state of which is no longer affected by the underlying alloy.[24,31] Intending to suppress the dealloying of Co, we performed another series of experiments for Pt−Co keeping the potential at 0.050 V during heating or cooling to a desired temperature. However, the critical temperature for the degradation was also the same (70 °C), which is also similar to the ORR experiments.[31] Hence, the operating temperature for Pt−Co may be limited to $t \leq 50$ °C.

4. Conclusions

The CO-tolerant HOR activities at the bulk Pt, Pt-skin layer on Pt−Co and Pt−Ru were investigated in 0.1 M $HClO_4$ solution at a practical temperature range from 30 to 90 °C for PEFCs. With the hydrodynamic voltammograms in the CFE, we determined the kinetically controlled current density (j_K) and k_{app} by correcting for the concentration of H_2 dissolved in the solution. The activation energies for the k_{app} were as low as 3.0, 4.2, and 5.3 kJ mol^{-1} at Pt, Pt−Co, and Pt−Ru, respectively. The j_K for the HOR at Pt decreased dramatically for $\theta_{CO} > 0.6$ at all temperatures, presumably due to a decrease in neighboring two-active (CO-free) sites required for H_2 dissociative adsorption in the rds. In contrast, the Pt−Ru and Pt−Co alloys showed excellent CO tolerance: the deceleration of CO adsorption rate

and very small reduction in j_K even at apparent high $\theta_{CO} = 0.6$. At low θ_{CO}, linearly adsorbed CO was dominant at the Pt−Co alloy electrode, whereas a large fraction of CO adsorbed on pure Pt in the bridged form, by which the HOR active sites were blocked more dramatically. Such a CO tolerance at Pt−Co and Pt−Ru was attributed to an electronic effect, which could weaken the Pt−CO interaction. The Pt−Co alloy, however, degraded once heated to 70 °C, due to the thickening of the Pt skin-layer, the electronic state of which is no longer affected by the underlying alloy.

Acknowledgment. This work was supported by the fund for "Leading Project; Next Generation Fuel Cells" of the Ministry of Education, Science, Culture, Sports and Technology of Japan.

Supporting Information Available: Calculation method of H_2 concentration dissolved in the solution and diffusion coefficient D from 30 to 90 °C; correction method of $[H_2]$, using diffusion-limiting current in the hydrodynamic voltammogram; calculation of CO concentration dissolved in the solution; and (4) supplementary data sets for Figure 7 (from 50 to 90 °C). This material is available free of charge via the Internet at http://pubs.acs.org.

References and Notes

(1) Vielstich, W.; Lamm, A.; Gasteiger, H. A., Eds. *Handbook of Fuel Cells*: *Fundamentals, Technology and Applications*; J. Wiley: New York, 2003.
(2) Lemons, R. A. *J. Power Sources* **1990**, *29*, 251.
(3) Igarashi, H.; Fujino, T.; Watanabe, M. *J. Electroanal. Chem.* **1995**, *391*, 119.
(4) Watanabe, M.; Motoo, S. *J. Electroanal. Chem.* **1975**, *60*, 275.
(5) Watanabe, M.; Motoo, S. *J. Electroanal. Chem.* **1976**, *69*, 429.
(6) Watanabe, M.; Motoo, S. *Denki Kagaku* **1976**, *44*, 602 (presently *Electrochemistry*).
(7) Watanabe, M.; Motoo, S. *J. Electroanal. Chem.* **1980**, *110*, 103.
(8) Watanabe, M.; Motoo, S. *J. Electroanal. Chem.* **1980**, *110*, 261.
(9) Watanabe, M.; Motoo, S. *J. Electroanal. Chem.* **1985**, *187*, 161.
(10) Watanabe, M.; Motoo, S. *J. Electroanal. Chem.* **1985**, *194*, 275.
(11) Ross, P. N.; Kinoshita, K.; Scarpellino, A. J.; Stonehart, P. *J. Electroanal. Chem.* **1975**, *59*, 177.
(12) Ross, P. N.; Kinoshita, K.; Scarpellino, A. J.; Stonehart, P. *J. Electroanal. Chem.* **1975**, *63*, 97.
(13) Gasteiger, H. A.; Markovic, N.; Ross, P. N., Jr.; Cairns, E. J. *J. Phys. Chem.* **1994**, *98*, 617.
(14) Gasteiger, H. A.; Markovic, N.; Ross, P. N., Jr. *J. Phys. Chem.* **1995**, *99*, 8945.
(15) Grgur, B. N.; Zhuang, G.; Markovic, N.; Ross, P. N., Jr. *J. Phys. Chem. B* **1997**, *101*, 3910.
(16) Ley, K. L.; Liu, R. X.; Pu, C.; Fan, Q. B.; Leyarovska, N.; Segre, C.; Smotkin, E. S. *J. Electrochem. Soc.* **1997**, *144*, 1543.
(17) Mukerjee, S.; Urian, R. C.; Lee, S. J.; Ticianelli, E. A.; McBeen, J. *J. Electrochem. Soc.* **2004**, *151*, A1094.
(18) Gonzalez, E. R.; Ticianelli, E. A. *J. Electroanal. Chem.* **2005**, *575*, 53.
(19) Sugimoto, W.; Saida, T.; Takasu, Y. *Electrochem. Commun.* **2006**, *8*, 411.
(20) Fujino, T. Thesis for M. Eng, Yamanashi University, 1996.
(21) Watanabe, M.; Igarashi, H.; Fujino, T. *Electrochemistry* **1999**, *67*, 1194.
(22) Watanabe, M.; Zhu, Y.; Uchida, H. *J. Phys. Chem. B* **2000**, *104*, 1762.
(23) Watanabe, M.; Zhu, Y.; Igarashi, H.; Uchida, H. *Electrochemistry* **2000**, *68*, 244.
(24) Igarashi, H.; Fujino, T.; Zhu, Y.; Uchida, H.; Watanabe, M. *Phys. Chem. Chem. Phys.* **2001**, *3*, 306.
(25) (a) Watanabe, M.; Wakisaka, M.; Uchida, H. *The 209th Meeting of the Electrochemical Society*, Abstract 243; May 7−12, 2006, Denver CO. (b) Wakisaka, M.; Mitsui, S.; Hirose, Y.; Kawashima, K.; Uchida, H.; Watanabe, M. *J. Phys. Chem. B*, in press, DOI: 10.1021/jp0653510.
(26) Wan, L. J.; Moriyama, T.; Ito, M.; Uchida, H.; Watanabe, M. *Chem. Commun.* **2002**, 58.
(27) Uchida, H.; Ozuka, H.; Watanabe, M. *Electrochim. Acta* **2002**, 47, 3629.
(28) Schmidt, T. J.; Gasteiger, H. A.; Stäb, D. D.; Urban, P. M.; Kolb, D. M.; Behm, R. J. *J. Electrochem. Soc.* **1998**, *145*, 2354.
(29) Schmidt, T. J.; Gasteiger, H. A.; Behm, R. J. *J. Electrochem. Soc.* **1999**, *146*, 1296.
(30) Wakabayashi, N.; Takeichi, M.; Itagaki, M.; Uchida, H.; Watanabe, M. *J. Electroanal. Chem.* **2005**, *574*, 339.
(31) Wakabayashi, N.; Takeichi, M.; Uchida H.; Watanabe, M. *J. Phys. Chem. B* **2005**, *109*, 5836.
(32) Yano, H.; Higuchi, H.; Uchida, H.; Watanabe, M. *J. Phys. Chem. B* **2006**, *110*, 16544.
(33) Watanabe, M.; Motoo, S. *J. Electroanal. Chem.* **1975**, *60*, 259.
(34) Uchida, H.; Ikeda, N.; Watanabe, M. *J. Electroanal. Chem.* **1997**, *424*, 5.
(35) Levich, V. G. In *Physicochemical Hydrodynamics*; Prentice Hall, Englewood Cliffs, NJ, 1962; p 112.
(36) Conway, B. E.; Tilak, B. V. *Electrochim. Acta* **2002**, *47*, 3571.
(37) Kunimatsu, K.; Uchida, H.; Osawa M.; Watanabe, M. *J. Electroanal. Chem.* **2006**, *587*, 299.
(38) Yajima, T.; Uchida, H.; Watanabe, M. *J. Phys. Chem. B* **2004**, *108*, 2654.
(39) Watanabe, M.; Motoo, S. *J. Electroanal. Chem.* **1986**, *206*, 197.
(40) Chang, S.-C.; Leung, L.-W. H.; Weaver, M. J. *J. Phys. Chem.* **1989**, *93*, 5341.
(41) Zhu, Y.; Uchida, H.; Watanabe, M. *Langmuir* **1999**, *15*, 8757.
(42) Breiter, B. W. *J. Electroanal. Chem.* **1975**, *65*, 623.
(43) Jambunathan, K.; Hillier, A. C. *J. Electroanal. Chem.* **2002**, *524*−*525*, 144.